A quantum logic gate for free electrons

Stefan Löffler[1], Thomas Schachinger[1,2], Peter Hartel[3], Peng-Han Lu[4,5], Rafal E. Dunin-Borkowski[4], Martin Obermair[6], Manuel Dries[6], Dagmar Gerthsen[6], and Peter Schattschneider[1,2]

[1]University Service Centre for Transmission Electron Microscopy, TU Wien, Wiedner Hauptstraße 8-10/E057-02, 1040 Wien, Austria

[2]Institute of Solid State Physics, TU Wien, Wiedner Hauptstraße 8-10/E138-03, 1040 Wien, Austria

[3]CEOS Corrected Electron Optical Systems GmbH, Englerstraße 28, 69126 Heidelberg, Germany

[4]Ernst Ruska-Centre for Microscopy and Spectroscopy with Electrons (ER-C) and Peter Grünberg Institute, Forschungszentrum Jülich, 52425 Jülich, Germany

[5]RWTH Aachen University, Ahornstraße 55, 52074 Aachen, Germany

[6]Laboratorium für Elektronenmikroskopie (LEM), Karlsruher Institut für Technologie (KIT), Engesserstraße 7, 76131 Karlsruhe, Germany

The topological charge m of vortex electrons spans an infinite-dimensional Hilbert space. Selecting a two-dimensional subspace spanned by $m = \pm 1$, a beam electron in a transmission electron microscope (TEM) can be considered as a quantum bit (qubit) freely propagating in the column. A combination of electron optical cylinder lenses can serve as a universal device to manipulate such qubits at the experimenter's discretion. We set up a TEM probe forming lens system as a quantum gate and demonstrate its action numerically and experimentally. High-end TEMs with aberration correctors are a promising platform for such experiments, opening the way to study quantum logic gates in the electron microscope.

1 Introduction

Manipulating the electron's phase is a current topic in electron microscopy. On the one hand, wave front engineering promises better spatial resolution [1], novel beam splitters [2], improved sensitivity for particular applications such as spin polarized electronic transitions [3], or manipulating nanoparticles via electron vortex beams [4]. In many respects, the physics of electrons with topological charge is similar to that of photons in singular optics (for an overview see [5]). In particular, quantum logic gates based on photons with orbital angular momentum (OAM) have been successfully demonstrated (e.g. in [6]). Other aspects are unique to electrons, such as easy manipulation in magnetic fields, the extraordinary sub-nm resolution, or novel solid-state applications such as diffraction in chiral crystals [7]. On the other hand, the coherent control of the interaction of fast electrons with electromagnetic radiation, either via near fields in PINEM [8, 9], resonant cavities [10] or laser accelerators [11] leads to oscillations in the probability distribution of the electron's momentum and energy, allowing the compression of fast electron pulses below the femtosecond time scale. A similar phenomenon occurs when Landau states propagate in a magnetic field, giving rise to peculiar rotations [12–14].

The fascinating possibility to shape the phase of the electron wave [15] with special holographic masks or via interaction with electromagnetic fields has led to two proposals for building quantum gates for traveling free electrons. The first proposal [16] uses a device called mode converter (MC) that can transform a plane electron wave into one with topological charge [17, 18]. Recently, an alternative approach based on energy gain or loss processes using laser-driven near field interactions was proposed [19, 20]. Here, we show proof-of-principle experiments using a MC as a quantum $\sqrt{NOT}$ gate, demonstrating the feasibility of the first approach.

Stefan Löffler: stefan.loeffler@tuwien.ac.at

2 Theory

2.1 Basis states

In a two-state system, any two orthogonal states can be chosen as basis for constructing qubits. Preliminary experimental results show that vortex electrons — eigen modes of the angular momentum operator that are topologically protected and carry quantized OAM of integer multiples of $\hbar$ — are very stable during manipulation in the column of a microscope [18]. Therefore, a Hilbert space spanned by two vortex states with topological charge $m = \pm 1$ (and linear combinations thereof) is a good candidate for electron qubits.

We use the two Laguerre-Gauss (LG) modes $LG_{1,0}$ and $LG_{-1,0}$ as basis states [21]. In cylindrical coordinates (r, ϕ, z) they have the real-space representations

$$\begin{aligned} \langle \vec{r}|R\rangle &= LG_{1,0} = r\mathrm{e}^{\mathrm{i}\phi} \cdot f(r,z), \\ \langle \vec{r}|L\rangle &= LG_{-1,0} = r\mathrm{e}^{-\mathrm{i}\phi} \cdot f(r,z) \end{aligned} \tag{1}$$

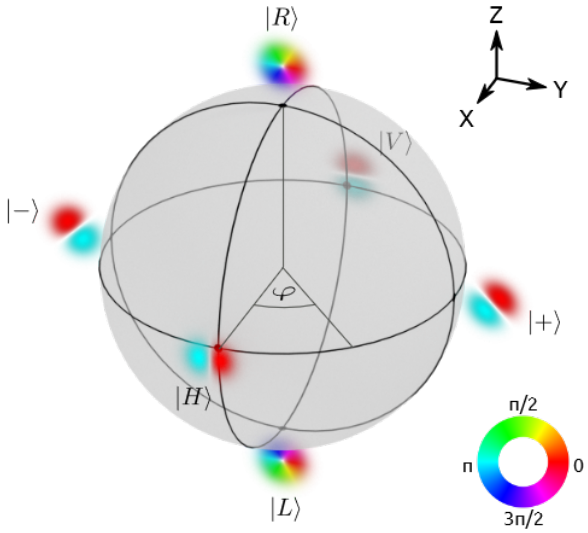

Figure 1: $|R\rangle$ and $|L\rangle$ states are represented by the north and south poles of the Bloch sphere. Also shown are the $|\pm\rangle$ and the $|H\rangle, |V\rangle$ states.

with

$$f(r,z) = \frac{A}{w(z)} \mathrm{e}^{-\frac{r^2}{w(z)^2}} \cdot \mathrm{e}^{\mathrm{i}\frac{kr^2}{2R(z)}} \cdot \mathrm{e}^{\mathrm{i}(kz - 2\zeta(z))},$$

where A is a real valued normalization factor. The waist $w(z) = w_0\sqrt{1+(z/z_R)^2}$ is the propagation dependent beam size, z_R is the Rayleigh length, k is the wave number, $R(z) = z(1+(z_R/z)^2)$ is the radius of the curvature of the wave front, and $\zeta(z) = \arctan(z_R/z)$ is the Gouy phase [1]. These are diffracting modes, i.e. the radial scale depends on the position z of the wave packet on the propagation axis. Note that z is considered here as a parameter used for propagation simulation. If not otherwise stated, the qubits are defined in the virtual or real focal planes $z = 0$. The two-dimensional Hilbert space spanned by $|R\rangle$ and $|L\rangle$ is conveniently presented as a Bloch sphere (Fig. 1). Similar to light optics, we define states

$$|H\rangle = \frac{1}{\sqrt{2}}(|R\rangle + |L\rangle) \qquad |V\rangle = \frac{1}{\sqrt{2}}(|R\rangle - |L\rangle) \quad (2)$$

and

$$|+\rangle = \frac{1}{\sqrt{2}}(|R\rangle + \mathrm{i}\,|L\rangle) \qquad |-\rangle = \frac{1}{\sqrt{2}}(|R\rangle - \mathrm{i}\,|L\rangle) \quad (3)$$

Performing qubit operations using a quantum logic gate requires three steps: preparation, manipulation using the gate, and readout, as sketched in Fig. 2.

[1] It has been pointed out that for non-relativistic electrons the Gouy phase depends on the time at which the propagating wave packet is observed [22], as $t = \langle z \rangle / v$ where v is the electron's speed.

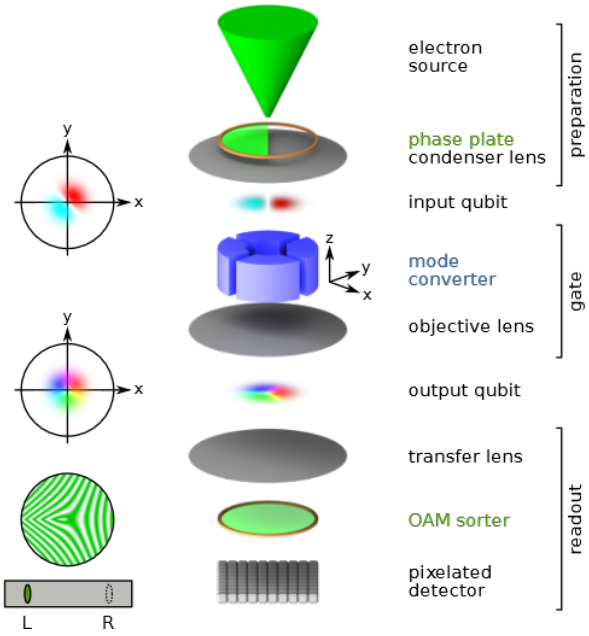

Figure 2: Column of an electron microscope with standard devices (black), phase shaping devices (green) and the qubit manipulator (blue). Electron qubits (color coded as in Fig. 1) travel down the z axis. Example of detecting the output qubit $|R\rangle$ of the $\sqrt{NOT}$ gate with an OAM sorter.

2.2 Qubit preparation

For preparing the input qubit, the electron beam is sent through a phase plate. For the proof-of-principle experiment, we prepare input qubits as states on the equator of the Bloch sphere

$$|I_\varphi\rangle = \frac{1}{\sqrt{2}}(|R\rangle + \mathrm{e}^{\mathrm{i}\varphi}\,|L\rangle) \quad (4)$$

with phase shift $\varphi \in [0, 2\pi)$. Using Eq. 1,

$$\langle \vec{r}\,|I_\varphi\rangle = \mathrm{e}^{\mathrm{i}\varphi/2}\sqrt{2}\, f(r,z)\, r\cos(\phi - \varphi/2). \quad (5)$$

Recalling the definition of Hermite-Gauss (HG) modes

$$HG_{1,0} = x f(r,z) \qquad HG_{0,1} = y f(r,z), \quad (6)$$

and $x = r\cos(\phi)$, Eq. 5 describes a $HG_{1,0}$ mode rotated by $\varphi/2$ in the (x, y) plane, apart of a global phase factor that is irrelevant for our purpose.

2.3 Qubit manipulation

Manipulation of qubits as prepared above on the Bloch sphere at the experimenter's discretion can be performed using a set of two quadrupoles (QPs) as used in a MC [16]. All (unitary) manipulations of a qubit correspond to a rotation on the Bloch sphere. In spherical coordinates, a general rotation by an angle θ around an axis given by the unit vector

$\vec{n} = (n_X, n_Y, n_Z)^\top$ corresponds to the unitary operator

$$\hat{R}_{\vec{n}}(\theta) = \mathrm{e}^{-\mathrm{i}\frac{\theta}{2}\vec{n}\cdot\vec{\sigma}} = \cos\left(\frac{\theta}{2}\right)\mathbb{1} - \mathrm{i}\sin\left(\frac{\theta}{2}\right)\vec{n}\cdot\vec{\sigma}. \quad (7)$$

where $\vec{\sigma}$ is the 3D vector of the Pauli matrices.

The MC performs a rotation of $\pi/2$ over the X axis of the Bloch sphere shown in Fig. 1

$$\mathbf{R}_X(-\pi/2) = \begin{pmatrix} \cos(\pi/4) & -\mathrm{i}\sin(\pi/4) \\ -\mathrm{i}\sin(\pi/4) & \cos(\pi/4) \end{pmatrix} = \frac{1}{\sqrt{2}}\begin{pmatrix} 1 & -\mathrm{i} \\ -\mathrm{i} & 1 \end{pmatrix}. \quad (8)$$

Apart from a global phase, this is a $\sqrt{NOT}$ quantum gate, usually abbreviated **RX**. Note that the axes X, Y, Z of the Bloch sphere in Fig. 1 must not be confounded with the axes x, y, z of the real space representation of the states, drawn in Fig. 2.

Applying the $\sqrt{NOT}$ gate to the input qubit using Eqs. 4 and 8 results in the output qubit

$$|O_\varphi\rangle \hat{=} \frac{1}{\sqrt{2}}\mathbf{RX}\begin{pmatrix} 1 \\ \mathrm{e}^{\mathrm{i}\varphi} \end{pmatrix} = \frac{1}{2}\begin{pmatrix} 1 - \mathrm{i}\mathrm{e}^{\mathrm{i}\varphi} \\ -\mathrm{i} + \mathrm{e}^{\mathrm{i}\varphi} \end{pmatrix} = \mathrm{e}^{\mathrm{i}(\frac{\varphi}{2} - \frac{\pi}{4})}\begin{pmatrix} \cos(\frac{\varphi}{2} - \frac{\pi}{4}) \\ -\sin(\frac{\varphi}{2} - \frac{\pi}{4}) \end{pmatrix} \quad (9)$$

It is readily apparent that for the eigen vectors of the transformation matrix, the trivial mapping occurs (see appendix), namely

$$|I_{0^\circ}\rangle = |H\rangle \mapsto \mathrm{e}^{-\mathrm{i}\pi/4}|H\rangle$$
$$|I_{180^\circ}\rangle = |V\rangle \mapsto \mathrm{e}^{\mathrm{i}\pi/4}|V\rangle.$$

2.4 Qubit readout

The third step is reading the output qubit. That means projecting it on the basis vectors of the Hilbert space, linked to a measurement device. Technically speaking, in the electron microscope these are pixels on a camera. This is a more subtle problem than it appears. As the intensity distribution of $|R\rangle$ and $|L\rangle$ in position space is identical (a ring), the two states cannot be distinguished and quantified by direct recording. Therefore, one of the OAM sorters proposed in the literature must be used, from early multi-pinhole interferometers [23] to holographic masks [24] to the more recent OAM unwrappers [25–28] which are based on a proposal for conformal mapping similar to light optics [29]. Their basis states — in the present case eigen states $|L\rangle, |R\rangle$ of the angular momentum operator L_z — become spatially separated in the sorter [2].

[2] Any readout basis can be selected by rotating the L_z basis of the measurement device on the Bloch sphere into the readout basis. In principle, this can be achieved with a second MC, exactly as described for qubit manipulation.

3 Experimental proof of principle

We performed a proof-of-principle experiment on the Jülich PICO microscope, which is a monochromated double-C_s-corrected (S)TEM instrument, together with numerical simulations of the beam propagation [30] to analyze the beam shape and phase in experimentally inaccessible planes such as the MC entrance and exit planes.

Electrons closely resembling HG modes can be produced by several means, e.g. by exploiting the Aharanov-Bohm effect of a magnetic rod [31]. Here, we used a Hilbert phase plate (HPP) [18, 32] inserted in the C3 aperture plane as a phase shifter for one half of an incident round beam, thereby preparing $|I_\varphi\rangle$ states (see appendix and [18]). These qubits were then sent through the MC realized by the C_s-corrector of the microscope [16, 18, 30]. All experiments were carried out at 200 keV.

We prepared a qubit

$$|I_{90^\circ}\rangle = \frac{1}{\sqrt{2}}(|R\rangle + \mathrm{i}|L\rangle) = |+\rangle, \quad (10)$$

rotating the x axis of the MC by $\varphi/2 = 45^\circ$ with respect to the HPP edge. According to Eq. 5 this is a $HG_{1,0}$ mode rotated by $\pi/4$. This qubit was sent through the MC, resulting in the gate action

$$|I_{90^\circ}\rangle \mapsto \mathbf{RX}|I_{90^\circ}\rangle = |R\rangle. \quad (11)$$

as given in Eq. 9.

Subsequently, the beam was sent through the objective lens and the projection system and was finally observed on a CCD.

A second experiment was performed with an input $HG_{1,0}$ mode rotated by $\varphi/2 = 65^\circ$ with respect to the x axis. According to Eq. 4 this corresponds to

$$|I_{130^\circ}\rangle = \frac{1}{\sqrt{2}}\begin{pmatrix} 1 \\ -0.643 - 0.766\,\mathrm{i} \end{pmatrix}. \quad (12)$$

The $\sqrt{NOT}$ gate performs

$$|I_{130^\circ}\rangle \mapsto \mathbf{RX}|I_{130^\circ}\rangle = \frac{\mathrm{e}^{\mathrm{i}\cdot 20^\circ}}{\sqrt{2}}\begin{pmatrix} 1.329 \\ -0.484 \end{pmatrix}. \quad (13)$$

Fig. 3 shows a comparison between the experimental beam in the sample plane and the corresponding simulation of propagation through the column. OAM analysis of the output qubits was done numerically [3] by first applying a polar transform $(x, y) \mapsto (r, \varphi)$ and a subsequent Fourier transform $\varphi \mapsto m$ [33]. The results are shown as histogram in Fig. 3. It is clearly visible that (apart from some impurities due to HPP imperfections [18, 30]) the output qubit in the $\varphi/2 = 45^\circ$

[3] OAM sorters have been tested successfully elsewhere [25–28]. Since the implementation of a sorter in the Jülich PICO microscope is currently not feasible we chose a numerical approach.

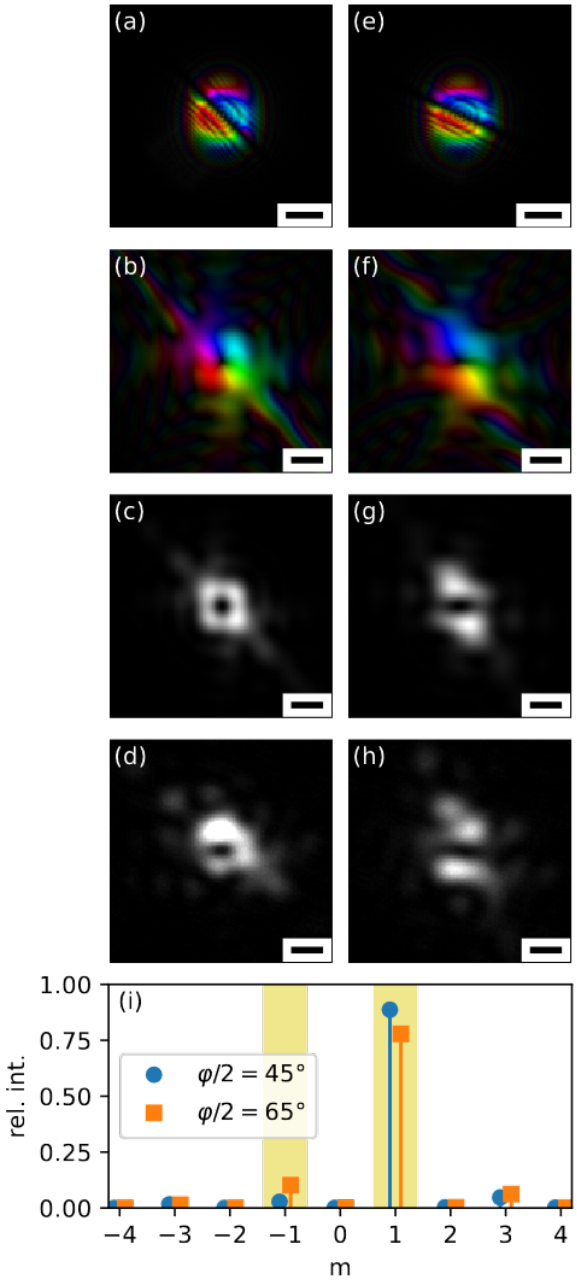

Figure 3: (a) Simulated input qubit for $\varphi/2 = 45°$. (b) Simulated output qubit after sending the input qubit (a) through the gate. (c) Intensity distribution of (b). (d) Experimentally observed intensity corresponding to (c). (e–h) Analogous data for $\varphi/2 = 65°$. (i) Intensity histogram for different OAM eigenvalues for the two output qubits. The scale bars in (a, e) denote 500 nm, all other scale bars denote 2 nm.

case consists essentially of the $m = 1$ component (corresponding to $|R\rangle$), whereas in the $\varphi/2 = 65°$ case, the output qubit features roughly $(-0.484/\sqrt{2})^2 \approx 0.12$ relative intensity of the $m = -1$ component (corresponding to $|L\rangle$) over the impurity background.

4 Discussion and Conclusion

High-end TEMs — instruments of utmost stability, spatial and energy resolution, sophisticated lens systems, ultra sensitive detectors and pulsed electron sources with repetition rates of the order of MHz — provide an ideal scenario to extend qubit manipulation from photons, superconducting circuits or ions to freely floating electrons. This novel platform for the study of qubits has several genuine features: qubits can be tailored from nm to µm size; in vacuum, they are topologically protected [34]; there is no need for cryogenic temperatures; they reveal high decoherence times and essentially no relaxation because the energies of the basis states are identical. The most attractive aspect is perhaps a broad range of tunable perturbations of the qubits via controlled interaction with electromagnetic radiation or matter on their way down the microscope column, in order to study the robustness of quantum gate operations, their quality and reliability [20]. Recent work on entanglement in electron microscopy [35–37] could provide opportunities for 2-qubit gates in non-separable systems.

Acknowledgements

PS thanks D. Karlovets and P. Hommelhof for valuable comments. SL, TS, and PS gratefully acknowledge financial support by the Austrian Science Fund under the projects P29687-N36 and I4309-N36. CEOS GmbH has received funding from the European Union's Horizon 2020 research and innovation programme under grant agreement No. 823717-ESTEEM3. PHL and REDB acknowledge the funding from European Union's Horizon 2020 research and innovation programme under grant agreement No. 856538 ("3D MAGiC"). MO, MD and DG acknowledge funding of this work by the German Research Foundation (Deutsche Forschungsgemeinschaft) under contract Ge 841/26. The authors acknowledge TU Wien Bibliothek for financial support through its Open Access Funding Programme.

A Hilbert phase plate

Fig. 4 shows a TEM image of the used HPP together with its action (i.e., producing the $|H\rangle$ state) when the quantum gate is switched off.

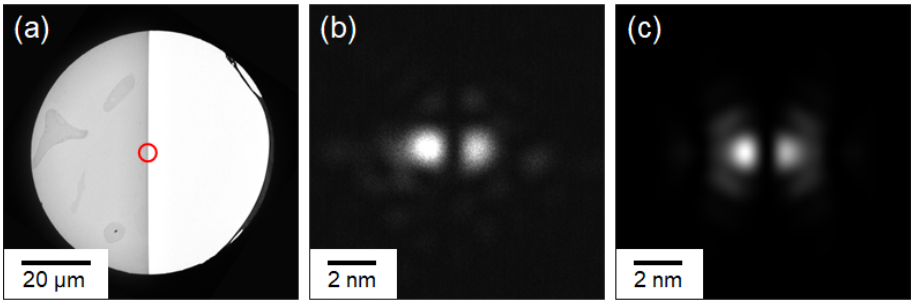

Figure 4: (a) TEM image of the Hilbert phase-plate (HPP) consisting of a aC/ZAC/aC layer system that is covering one half of a 70 µm aperture. The HPP was installed in the C3 aperture plane of the PICO microscope, with the red circle marking the actual illuminated area. (b) Experimental image of the (unrotated) qubit with inactive quantum gate. (c) Numerical simulation corresponding to (b).

B Trivial mapping of $|H\rangle$ and $|V\rangle$

Fig. 5 shows experimental and simulated data for the (trivial) action of the quantum gate on $|H\rangle$ and $|V\rangle$.

References

[1] E. Rotunno, A.H. Tavabi, E. Yucelen, S. Frabboni, R.E. Dunin Borkowski, E. Karimi, B.J. McMorran, and V. Grillo. Electron-beam shaping in the transmission electron microscope: Control of electron-beam propagation along atomic columns. *Physical Review Applied*, 11 (4):044072, April 2019. DOI: 10.1103/physrevapplied.11.044072.

[2] J. Hammer, S. Thomas, P. Weber, and P. Hommelhoff. Microwave chip-based beam splitter for low-energy guided electrons. *Physical Review Letters*, 114(25):254801, 2015. DOI: 10.1103/PhysRevLett.114.254801.

[3] T. Schachinger, S. Löffler, A. Steiger-Thirsfeld, M. Stöger-Pollach, S. Schneider, D. Pohl, B. Rellinghaus, and P. Schattschneider. EMCD with an electron vortex filter: Limitations and possibilities. *Ultramicroscopy*, 179:15–23, 2017. DOI: 10.1016/j.ultramic.2017.03.019.

[4] J. Verbeeck, H. Tian, and G. Van Tendeloo. How to manipulate nanoparticles with an electron beam? *Advanced Materials*, 25(8):1114–1117, 2013. DOI: 10.1002/adma.201204206.

[5] S. Franke-Arnold, L. Allen, and M. Padgett. Advances in optical angular momentum. *Laser and Photonics Reviews*, 2(4):299–313, 2008. DOI: 10.1002/lpor.200810007.

[6] Amin Babazadeh, Manuel Erhard, Feiran Wang, Mehul Malik, Rahman Nouroozi, Mario Krenn, and Anton Zeilinger. High-dimensional single-photon quantum gates: Concepts and experiments. *Phys. Rev. Lett.*, 119:180510, Nov 2017. DOI: 10.1103/PhysRevLett.119.180510.

[7] Roeland Juchtmans, Armand Béché, Artem Abakumov, Maria Batuk, and Jo Verbeeck. Using electron vortex beams to determine chirality of crystals in transmission electron microscopy. *Phys. Rev. B*, 91:094112, Mar 2015. DOI: 10.1103/PhysRevB.91.094112.

[8] G. M. Vanacore, I. Madan, G. Berruto, K. Wang, E. Pomarico, R. J. Lamb, D. McGrouther, I. Kaminer, B. Barwick, F. J. Garcia De Abajo, and F. Carbone. Attosecond coherent control of free-electron wave functions using semi-infinite light fields. *Nature Communications*, 9(1):2694, 2018. DOI: 10.1038/s41467-018-05021-x.

[9] A. Feist, K.E. Echternkamp, J. Schauss, S.V. Yalunin, S. Schäfer, and C. Ropers. Quantum coherent optical phase modulation in an ultrafast transmission electron microscope. *Nature*, 521(7551):200–203, 2015. DOI: 10.1038/nature14463.

[10] C. Kealhofer, W. Schneider, D. Ehberger, A. Ryabov, F. Krausz, and P. Baum. All-optical control and metrology of electron pulses. *Science*, 352(6284):429–433, 2016. DOI: 10.1126/science.aae0003.

[11] N. Schönenberger, A. Mittelbach, P. Yousefi, J. McNeur, U. Niedermayer, and P. Hommelhoff. Generation and characterization of attosecond microbunched electron pulse trains via dielectric laser acceleration. *Physical Review Letters*, 123(26):264803, 2019. DOI: 10.1103/PhysRevLett.123.264803.

[12] K.Y. Bliokh, P. Schattschneider, J. Verbeeck, and F. Nori. Electron vortex beams in a magnetic field: A new twist on Landau levels and Aharonov-Bohm states. *Physical Review X*, 2(4):041011, 2012. DOI: 10.1103/PhysRevX.2.041011.

[13] Peter Schattschneider, Thomas Schachinger, Michael Stöger-Pollach, Stefan Löffler, Andreas Steiger-Thirsfeld, Konstantin Y. Bliokh, and Franco Nori. Imaging the dynamics of free-electron landau states. *Nature Communications*, 5:4586, August 2014. DOI: 10.1038/ncomms5586.